CrystEngComm

ROYAL SOCIETY OF CHEMISTRY

PAPER

View Article Online
View Journal | View Issue

Cite this: *CrystEngComm*, 2021, **23**, 741

Efficient photocatalytic degradation of methyl violet using two new 3D MOFs directed by different carboxylate spacers†

Jun Wang, *[a] Congying Rao,[b] Lu Lu,[a] Shile Zhang,[a] Mohd Muddassir [c] and Jianqiang Liu *[b]

Received 10th November 2020,
Accepted 23rd November 2020

DOI: 10.1039/d0ce01632b

rsc.li/crystengcomm

Two highly stable metal–organic frameworks (MOFs) assembled by a flexible 1,4-bis(2-methylimidazol-1-yl) butane (bib), and two different aromatic carboxylate coligands, namely, [Zn(BDC–OH_2)(bib)] (**1**) and [Cd_3(BTC)$_2$(bib)(DMF)$_3$] (**2**) (H_2BDC–OH_2 = 2,5-dihydroxyterephthalic acid, H_3BTC = 1,3,5-benzenetribenzoic acid), were designed and synthesized. **1** showed a 4-fold interpenetration of 4-connected dia-type topological net. In **2**, the 3D topological structure can be viewed as a (3,4,5)-connected network, and its Schläli point is $\{4{\cdot}6^2\}_2$ $\{4^2{\cdot}6{\cdot}8^3\}$ $\{4^6{\cdot}8^9\}$. Different auxiliary carboxylate ligands were examined with respect to the building of various structures. **1** and **2** have outstanding photocatalytic behaviors for the disintegration of methyl violet (MV) under UV irradiation.

Introduction

Organic aromatic dyes and heavy metal ions are widely applied in textiles, medicines, and other industries.[1–3] They are very harmful to humans due to their toxicity and carcinogenicity when these dyes are dumped into water. Recently, more and more technologies and strategies have been designed and explored to reduce and eliminate them.[4,5] Among these methods, photodegradation has been identified as one of the effective tools in eliminating such dyes.[6–9] Although many traditional semiconductors have been extensively used as photocatalysts to degrade organic dyes, there are certain defects (such as loss of reactivity, low efficiency and separation). Therefore, it is very urgent to develop a new catalytic material with high efficiency and friendly environment.[10] Metal–organic frameworks (MOFs) assembled from the metal ions/metal clusters and organic linkers are transferring from a focus on the structural feature to their various outstanding applications, including luminescent sensing, supercapacitor electrode, gas storage, and biomedical therapy.[11,12] Interestingly, the MOFs have been just recently used as the photocatalysts for dye degradation. However, the key factor in the building of promising MOFs is the design and synthesis of suitable organic ligands.[13] Flexible bis(imidazole) derivatives have been extensively explored in coordination chemistry because the imidazole rings are able to rotate freely around the –$(CH_2)_n$– (n = 2–8) group to satisfy the geometric requirement of the metal centers.[14] However, rigid and symmetric multicarboxylates have been designed and selected as linkers to construct unique and intriguing MOFs, which showed excellent properties due to their various coordination modes and π-conjugated skeleton.[15] Based on the background of this study, the selection and assembly of bis(imidazole)-based bridging ligand with 2,5-dihydroxyterephthalic acid and 1,3,5-benzenetribenzoic acid in the presence of Zn/Cd salts were explored. Differential structural aspects of the MOFs, namely, [Zn(BDC–OH_2)(bib)] (**1**) and [Cd_3(BTC)$_2$(bib)(DMF)$_3$] (**2**), clearly demonstrate the effect of these geometric configurations of the ligands and the coordination tendency of the metal cations. Herein, we tried to apply the effectiveness of **1** and **2** for the decomposition of methyl violet (MV) under UV irradiation with an underlying application from the purification viewpoint.

Photocatalytic method

The sample of **1** or **2** (40 mg) was dispersed in a 50 mL aqueous solution of methyl violet (10 mg L^{-1}) with stirring in the dark for 30 min to ensure the establishment of an adsorption–desorption equilibrium. The photocatalytic degradation of MV was conducted on an UV-400 type photochemical reactor having a mercury lamp of 100 W (mean wavelength = 365 nm). Aliquots of 5.0 mL were taken out at specific time intervals and separated through

[a] *School of Chemistry and Environmental Engineering, Sichuan University of Science & Engineering, Zigong, PR China. E-mail: scwangjun2011@126.com*
[b] *Key Laboratory of Research and Development of New Medical Materials of Guangdong Medical University, School of Pharmacy, Guangdong Medical University, Dongguan, 523808, China. E-mail: jianqiangliu2010@126.com*
[c] *Department of Chemistry, College of Science, King Saud University, Riyadh 11451, Saudi Arabia*

† Electronic supplementary information (ESI) available. CCDC 2021620 and 2021621. For ESI and crystallographic data in CIF or other electronic format see DOI: 10.1039/d0ce01632b

centrifugation and then subsequently analyzed using a UV spectrophotometer. Moreover, a control experiment was conducted under the identical conditions without adding the MOF-based catalysts **1** or **2**.

Results and discussion

[Zn(BDC–OH$_2$)(bib)] (1)

When the BDC–OH$_2$ ligand was used to react with the Zn(II) salt and bib, a new structure of **1** was obtained. It was revealed that **1** includes one Zn(II) ion, one BDC–OH$_2$ ligand and one bib linker (Fig. 1a). The Zn(II) atom is connected by two O atoms from different carboxyl groups from the two BDC–OH$_2$ ligands and two N atoms from the bib linkers, which can be deemed to be a tetrahedral subunit. Each BDC–OH$_2$ behaves in monodentate coordination mode and connects the metal centers to shape a wave-like 1D chain (Fig. S1 and Scheme S1a†), which is further joined by the bib ligands to generate a 3D net from two different directions (Fig. 1b and S2†). From the topological point of view, if each mononuclear subunit is treated as a 4-connected node, and BDC–OH$_2$ and bib linkers are considered as the linkages; the structural feature of **1** is a dia-type topology (Fig. 1c).[16] The 3D network of **1** possesses maximum dimensions (the longest intracage distances across the unit along the directions) of 31 × 26 × 16 Å^3. The cavity is large enough to be filled *via* the mutual entanglement of three independent equivalent nets, thus generating a [2 + 2] interpenetrating dia network belonging to class IIIa (Fig. 1d). Thus, **1** is 4-fold interpenetrating frames, which looks similar to that of the documented MOFs of [Zn$_4$(μ_4-O)(L1)6(DMF)$_2$][17] and [Zn$_4$(μ_4-O)(L2)$_3$] (H$_2$L1 = 6,6′-di-chloro-2,2′-diethoxy-1,10-binaphthyl-4,4′-dibenzoic acid and H$_2$L2 = 6,6′-dichloro-2,2′-dibenzyloxy-1,10-binaphthyl-4,4′-dibenzoic acid).[18] Compared to the MOF **1**, they have more flexible skeleton and low dimensional feature.

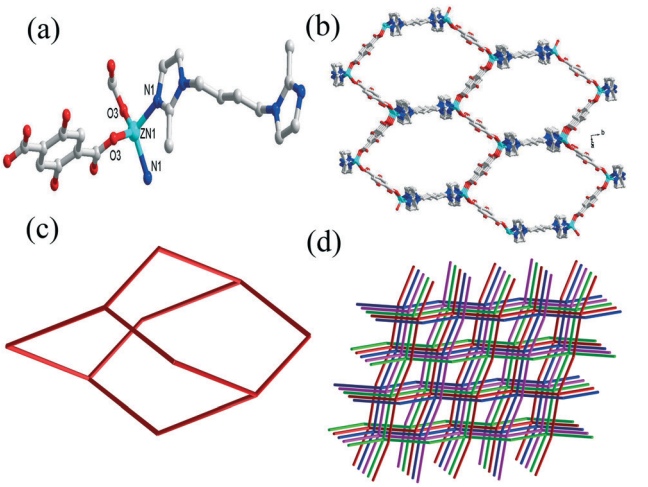

Fig. 1 (a) View of the coordination environment of Zn center; (b) 3D porous network; (c) the dia-type topological net; (d) view of the 3D 4-fold interpenetrated net.

[Cd$_3$(BTC)$_2$(bib)(DMF)$_3$] (2)

The above results prompted us to explore the highly connected topological types. Then, we used BTC instead of BDC–OH$_2$. It was revealed that the asymmetric unit of **2** comprises three Cd(II) cations, two BTC ligands, one bib ligand and three coordinated DMF molecules (Fig. 2a). The Cd1 ion is seven-coordinated with pentagonal bipyramid geometry and connected to 7 oxygen atoms of the four carboxyl groups from the four BTC linkers and one oxygen atom from the coordinated DMF molecule. The Cd2 ion is connected by four O atoms from three BTC, one O atom of the coordinated DMF molecule and one imidazole N atom directed from one bib, thus exhibiting a slightly distorted octahedral geometry. Cd3 is an octahedral geometry, being connected by four O atoms from the two BTC linkers, one O atom from a coordinated DMF and one imidazole N atom from one bib. In **2**, the BTC shows one coordination mode and acts as a μ_5-bridging linkage to join five Cd centers (Scheme S1b†). Two of these carboxyl groups coordinate to four metal centers (two Cd1 and two Cd2) with μ_2–η^1:η^2 mode, thus generating a dinuclear subunit. The third group showing μ_1–η^1:η^1 mode binds to one adjacent Cd center. Then, the Cd centers are further linked by BTC to shape a 3D coordination framework (Fig. 2b and S3†). The bib ligands adopt *anti*-conformation and are inserted in the pore (Fig. 2b). To allow a better visual connection of **2**, the dinuclear subunits are encompassed by the four BTC^{3-} and one bib linker, which are recorded as 5-connected nodes. Cd3 centers are besieged by two BTC^{3-} and one bib linker, which can simply be regarded as 3-connected nodes. The full 3D topological structure of **2** is a (3,4,5)-connected net; its Schläli point is $\{4{\cdot}6^2\}_2$ $\{4^2{\cdot}6{\cdot}8^3\}$ $\{4^6{\cdot}8^9\}$ (Fig. 1e).[19] PLATON calculation manifested that the full solvent-accessible volume accounts for about 10% of the total volume in **2**.[20,21]

Through the above structural analysis of **1** and **2** adopt new abilities for tuning the network topologies by controlling the length and skeleton of the linkages. In **2**, Cd centers are bridged by the triangular BTC and bidentate bib at three dimensions, which resulted in a 3D non-interpenetrated motif. By shortening the straight tricarboxylate from BTC to BDC accompanied by an alternation of Cd^{2+} to Zn^{2+} with smaller atomic radius, the corresponding **1** induced the high connectivity of these frames to cut down 5-c to 4-c.[22] Thus, the full networks can be regulated by the character of ligand and geometry of metal center. The channels are occupied by disordered DMF and water molecules. About 22% of solvent-accessible volume is estimated using PLATON. Note that the pores of the channels may be partly blocked by the DMF molecules and methyl groups from bib molecules and the actual pore sizes are less than 7.5 × 4.1 A^3.

Physical property of 1–2

The UV-vis spectra in the solid-state at room temperature were measured for **1–2** (Fig. S4†). The maximum absorption

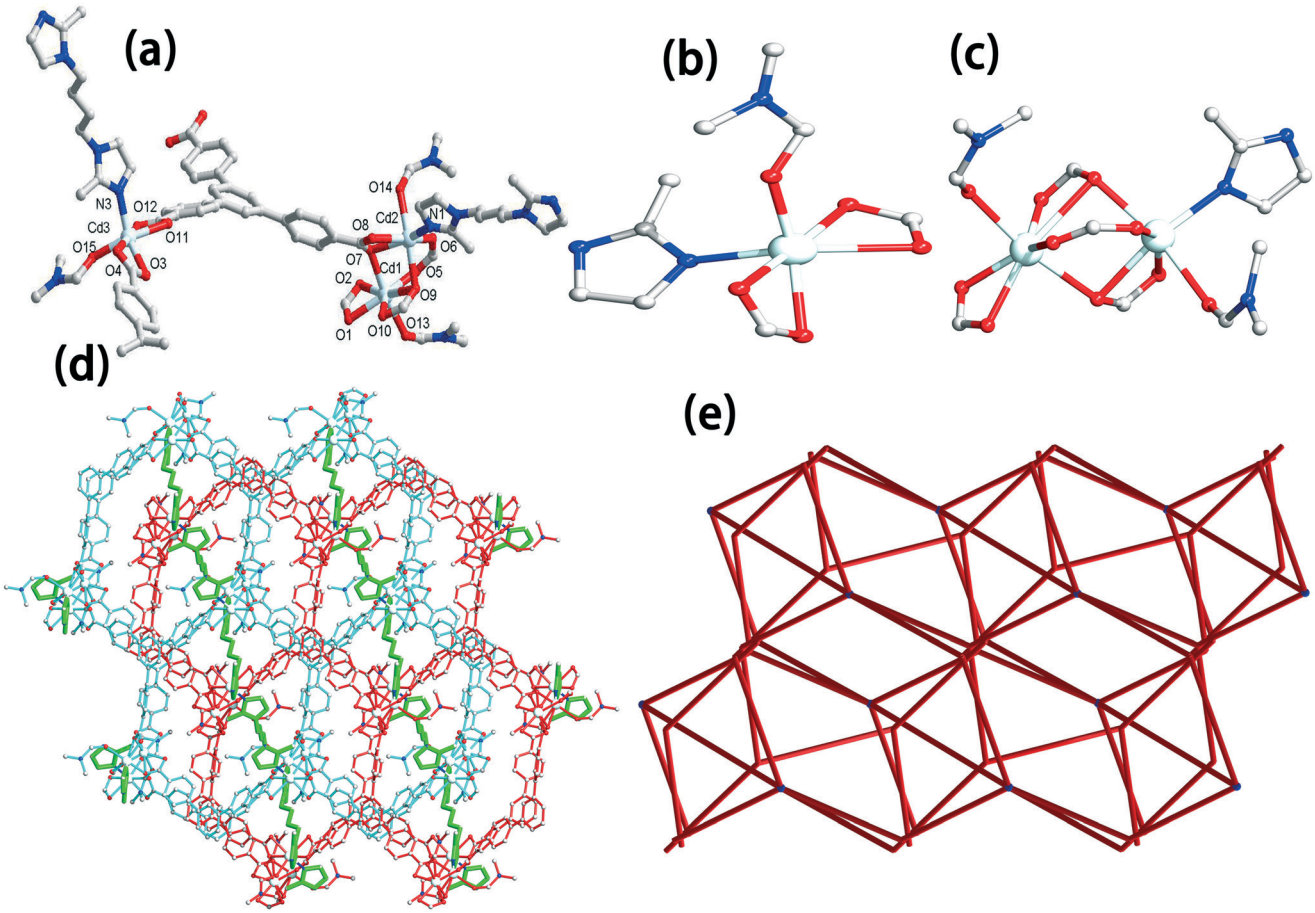

Fig. 2 (a) Coordination environment around the Cd^{2+} centers in **2**. (b) and (c) The two different Cd-based SBUs; (d) a 3D structure formed by $[(Cd(BTC)_4]_n$ and [Cd(bib)] chain unit. (e) (3,4,5)-Connected diagrammatic drawing.

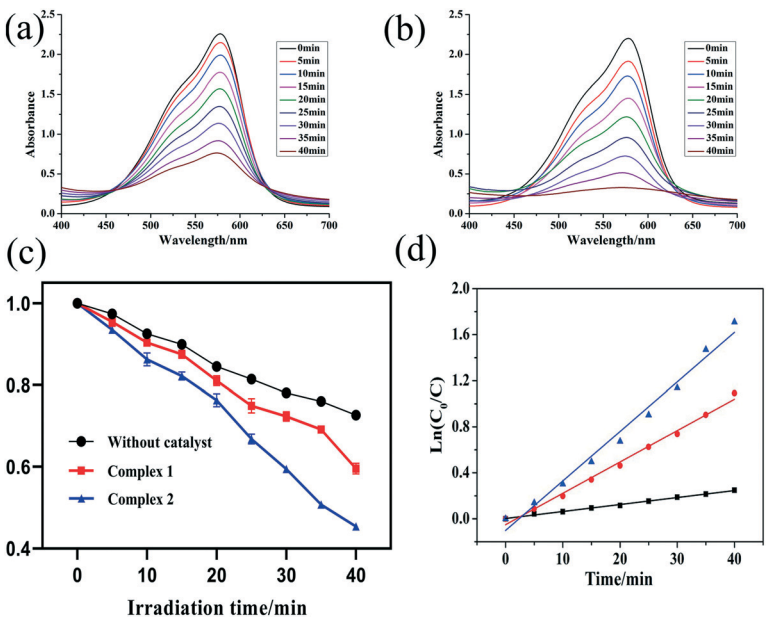

Fig. 3 (a) and (b) Electronic absorption spectra of the MV solution on UV irradiation in presence of photocatalysts **1** and **2**, respectively; (c) experiment results of the catalytic degradation of MV dye; (d) linear-fitting function plot.

peaks of **1–2** were observed at *ca.* 284 and 303 nm. The absorption results were fitted by the Kubelka–Munk function. The energy band gaps were obtained *ca.* 3.27 eV for **1** and 2.28 eV for **2** through the extrapolation of the linear part of absorption edges. These band gap values suggested **1** and **2** may have the potential advantages and characteristics for photocatalytic performance.[23]

Photocatalytic properties of MOFs 1 and 2

We have used methyl violet (MV) as the typical contaminant in water to estimate the catalytic efficiencies of **1–2** under UV irradiation. The absorption peaks of MV were remarkably decreased in the presence of **1–2** within 40 min. Note that the peaks declined dramatically at the same condition in the presence of catalyst **2** (Fig. 3a and b).[24] The variations of C/C_o *vs.* irradiation time for **1–2** were plotted (Fig. 3c).

The results are displayed as changes in the C/C_0 plot of the MV solution *versus* the irradiation time (Fig. 3c). Compared to the control group with 24.87% (without catalyst), the photocatalytic activity increased from 66.45% and 85.19% in the presence of pure **1** and **2** after 40 min irradiation, respectively. Based on the current reactive rates and efficiencies, it was indicated that the photocatalytic activity of **2** surpasses **1**. This may be attributed to the relatively low capture capability for MV due to its entanglement feature and weak conjugated system of **1**.[25,26] The rate constants for the MV photodegradation in the presence of the photocatalysts **1** and **2** were 0.0272 (10) min^{-1} and 0.0431 (2) min^{-1}, respectively (Fig. 3d). We have also explored the effect of the particle size in the photocatalytic performance and found that the size had little impact on the photocatalytic activity of **1** and **2**.

We have explored the plausible mechanism of MV by **2**, the catalytic exploration experiments were implemented before three types of scavengers were added.[27,28] It is obvious that these values fall rapidly from 85.19% to 82.1%, 50.2% and 83.2% (Fig. 4a and b). Three types of scavengers, including tertiary butyl alcohol (TBA), benzoquinone (BQ), and ammonium oxalate (AO), can act as hydroxyl radicals ($HO^{\bullet}$), superoxide radicals ($O_2^{\bullet-}$) and leaving holes (h^+), respectively. Thus, the data showed that $O_2^{\bullet-}$ was the main active species, while $^{\bullet}OH$ and h^+ may contribute to the MV degradation. The relevant rate constant (k) for the deterioration of MV in **2** was found to reduce from 0.0431 (2) to 0.0173 (6) min^{-1} in the presence of BQ (Fig. 4c and Table S3†). This inhibiting effect from BQ is also presented in polymer **1**.

Based on previous research and current experimental results, the catalytic degradation mechanism can be inferred. The MOF **2** has successful supplied photon transitions with equivalent or higher the band gap (2.86 eV) when skeleton was irradiated; then the electrons get excited from the valence band (VB) to the conduction band, impressing the holes in the valence band. The photoexcited hole electrons have the ability to oxidize the dyes or can react with OH^- to generate OH. These $^{\bullet}OH$ species can straightway oxidize these dyes and effectively break them down to finish the full catalytic process (Scheme 1).[29,30] Furthermore, to explore the stability of these catalytic materials as photocatalysts, we

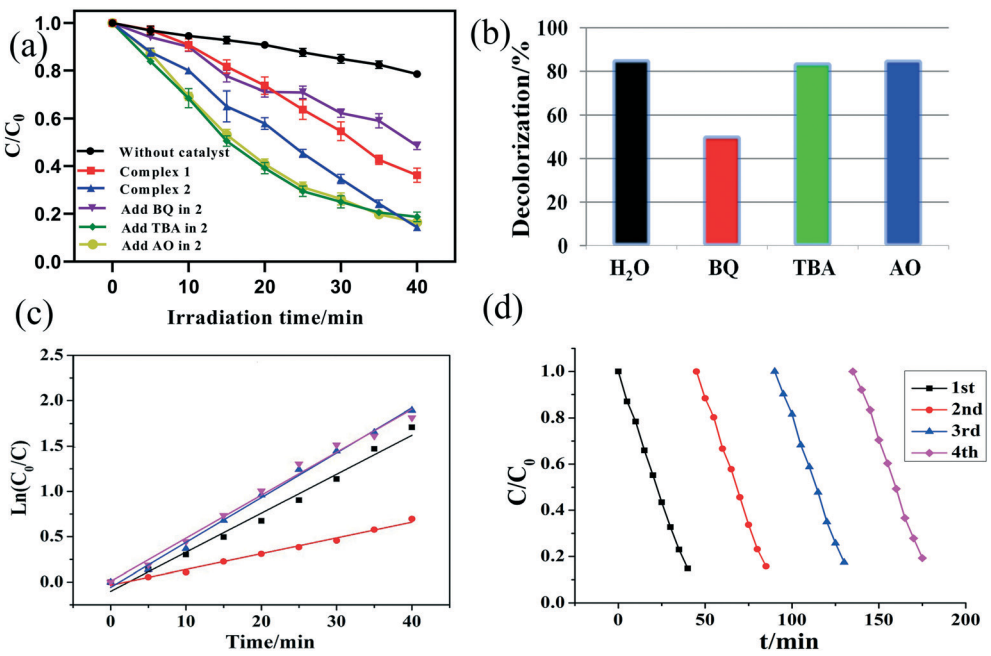

Fig. 4 (a) and (c) photodegradation of the MV solution in the different scavenger solutions in **2**; (b) the plot as a function of deduced mechanism of the degradation of MV by **2**; (d) cycling runs of the photocatalytic degradation of MV in **2**.

repeated the experiment four times under the same conditions (Fig. 4d). The results showed that the catalytic properties of these materials did not change significantly, which indicates that the materials are very stable and recyclable.[31,32] We also investigated the morphological changes of the samples before and after catalysis, SEM experiments show that the external morphology of the samples has little change (Fig. S9†).

Compared with the catalytic performances of the reported Zn/Cd-based MOFs (Table 1),[33] **2** has excellent photocatalytic degradation of MV. Although some of them showed good efficiency for the degradation of MV, the photocatalysts had large dosage and the concentration of MV was higher than that of this work.

Identification of the degradation products of MV dye

The degradation products were analyzed by LC-MS and the fragmented products were evaluated by the mass fragmentation pattern.[34,35] From the MS fragmentation pattern, the *m*/*z* values were achieved and these values correspond to the degradation products obtained during the photodegradation of MV (Fig. S10†). Hence, from the *m*/*z* values, the degradation products were traced and probable mechanistic pathway for the degradation of MV dye was suggested (Scheme 2). A low intensity signal was obtained at *m*/*z* = 358, which corresponds to the molar mass of MV. The intensity of this signal and the simultaneous appearance of multiple mass signals predicted that the degradation of MV took place. Two types of degradation patterns were predicted for MV according to the *m*/*z* signals obtained from the MS pattern. Firstly, MV undergo degradation to give signals at *m*/*z* = 344 and 330. This fragment (*m*/*z* = 316) undergoes further degradation to give multiple signals at *m*/*z* = 301 and 300. The degradation products corresponding to these multiple signals were identified and a mechanistic pathway for the degradation of MV was suggested. However, in the second case, MV degraded to give signal at *m*/*z* = 301 and underwent further degradation to form multiple signals at *m*/*z* = 181, 168 and 124.

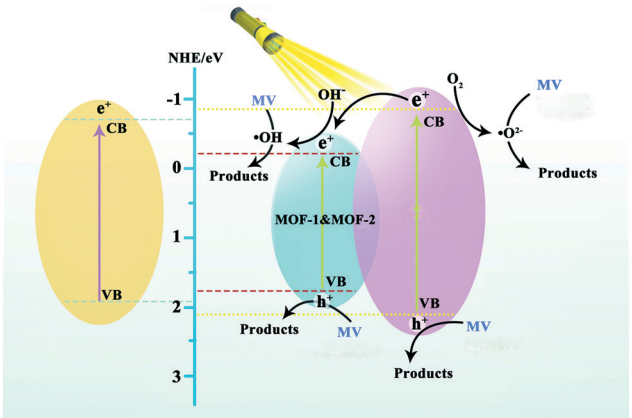

Scheme 1 The possible schematic mechanism between the energy transition and the active species for degradation of MV.

Conclusions

Two new d^{10}-based MOFs constructed from the flexible bis(imidazole) derivative 1,4-bis(2-methylimidazol-1-yl)butane (bib) ligand with linear dicarboxylate and angular tricarboxylic acid were successfully obtained. Structural differences in **1** and **2** indicate that the multicarboxylate ligands play an important role in the coordination mode and in the final structure. **2** displays efficient photodegradation of MV. The mechanistic investigation indicates that the main active component is the superoxide radicals ($O_2^{-\bullet}$). The intermediate products and degradation pathway of MV were discussed based on the results of LC-MS. It can be concluded that **1**–**2** can be used as potential photocatalysts.

Table 1 List of Zn^{II}/Cd^{II}-based materials for the degradation of dye MV

Formula	Ligands	Light source	Efficiency (%)	Ref.
[Zn(L)]	H_2L = 1,4-bis(triazol-1-yl)terephthalic acid	UV	61	33*a*
$[Zn_5(L)_2(DMF)_2(\mu_3\text{-}H_2O)]$	H_5L = 3,5-di(3′,5′dicarboxylphenyl)benzoic acid	UV	73	33*b*
$[Zn_4(NDC)_{3.5}(\mu_4\text{-}OH)(DMF)]$	H_2NDC = 1,4-naphthalenedicarboxylic acid	UV	78	33*c*
$[Zn_2(L)(DMF)_3]$	H_4L = terphenyl-3,3″,5,5″-tetracarboxylic acid	UV	72	33*d*
$[Zn(L)(4,4'\text{-bipy})_4]$	H_2L = 1,4-bis(3-carboxylbenzyl)piperazine acid	UV	68	33*e*
$[Cd(H_2L)(bpz)]$	H_4L = 5,5′-(1,4-phenylenebis(methyleneoxy))diisophthalic acid and bpz = 3,3′,5,5′-tetramethyl-4,4′-bipyrazole	UV	77	33*f*
$[Cd_2(H_4L)(L)(bpz)_2]$	H_4L = 5,5′-(1,4-phenylenebis(methyleneoxy))diisophthalic acid	UV	44	33*g*
$Cd(dbp)(H_2O)]$	H_2dbp = 4′-(4-(3,5-dicarboxylphenoxy)phenyl)-4,2′:6′,4′-terpyridine	UV	93	33*h*
[Cd(L)(bb)]	H_2L = 3,3′-[{1,3-phenylenebis-(methyleneoxy)}dibenzoic acid]; bb = 4,4′-bis(imidazolyl) biphenyl	UV	72	33*i*
$[Zn(BDC\text{–}OH_2)(bib)]$	Bib = 1,4-bis(2-methylimidazol-1-yl)butane and $H_2BDC\text{–}OH_2$ = 2,5-dihydroxyterephthalic acid and	UV	66	This work
$[Cd_3(BTC)_2(bib)(DMF)_3]$	H_3BTC = 1,3,5-benzenetribenzoic acid	UV	85	This work

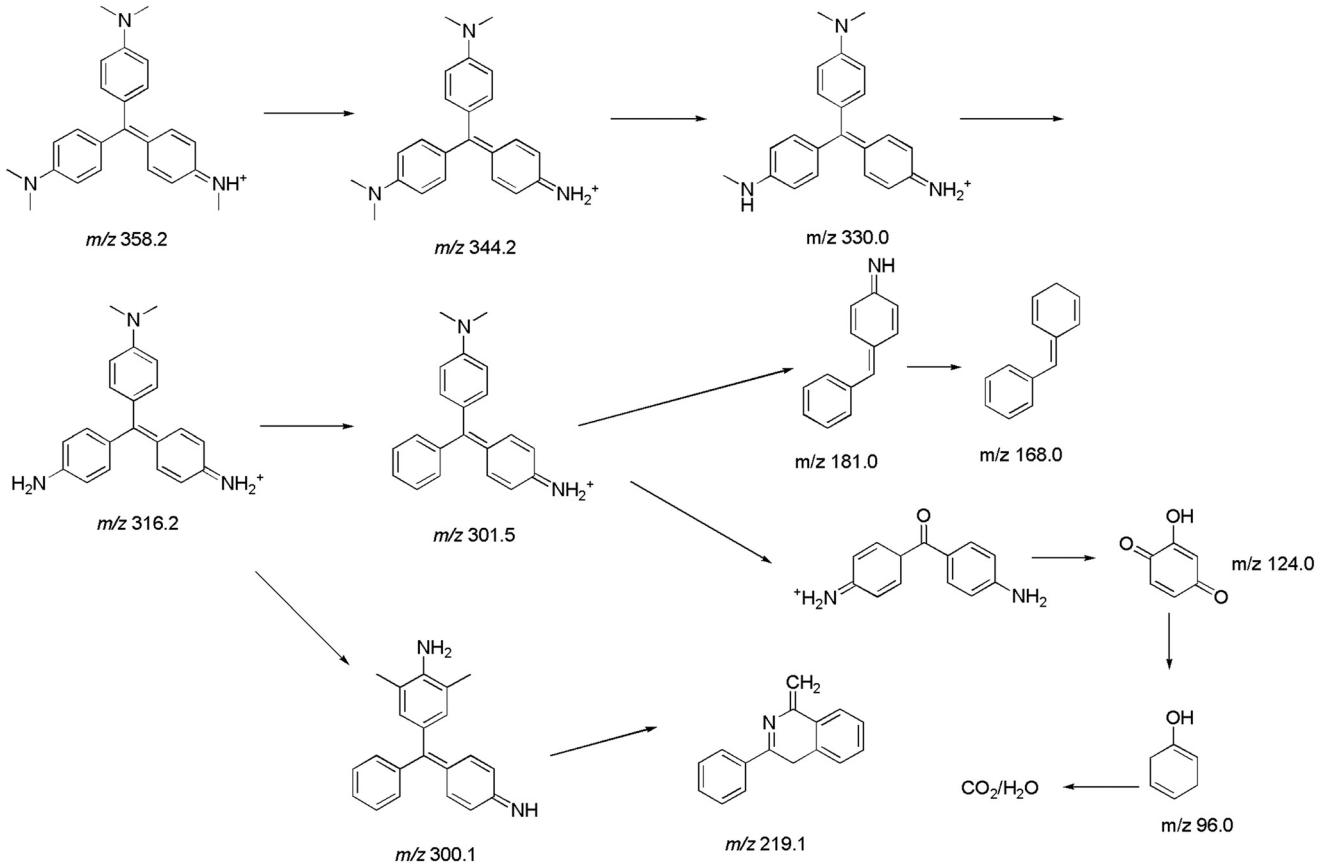

Scheme 2 Photodegradation pathway of MV dye and trace of the degradation products.

Conflicts of interest

The authors declare no competing financial interest.

Acknowledgements

The authors acknowledge financial assistance from Sichuan University of Science and Engineering (no. 2019RC21), the Project of Zigong Science & Technology (No. 2019YYJC06), the Open Project Program of Chemical Synthesis and Pollution Control Key Laboratory of Sichuan Province (CSPC202008) and the Education Committee of Sichuan Province (No. 17ZA0275) and Dr. Mohd. Muddassir is grateful to Researchers Supporting Project number (RSP-2020/141), King Saud University, Riyadh, Saudi Arabia, for financial assistance and Guangdong University Youth Innovation Talent Project (2020KQNCX024).

References

1 A. P. Vieira, S. A. A. Santana, C. W. B. Bezerra, H. A. S. Silva, J. A. P. Chaves, J. C. P. Melo, E. C. S. Filho and C. Airoldi, *Chem. Eng. J.*, 2011, **173**, 334–340.

2 (*a*) L. Qin, H. Z. Chen, J. Lei, Y. Q. Wang, T. Q. Ye and H. G. Zheng, *Cryst. Growth Des.*, 2017, **17**, 1293–1298; (*b*) J. Q. Liu, G. P. Li, W. C. Liu, Q. L. Li, B. H. Li, R. W. Gable, L. Hou and S. R. Batten, *ChemPlusChem*, 2016, **81**, 1299–1304.

3 (*a*) X. J. Huang, *J. Alloys Compd.*, 2017, **690**, 356–359; (*b*) L. Esrafili, F. D. Firuzabadi, A. Morsali and M. L. Hu, *J. Hazard. Mater.*, 2021, **403**, 123696.

4 M. E. Russo, F. D. Natale, V. Prigione, V. Tigini, A. Marzocchella and G. C. Varese, *Chem. Eng. J.*, 2010, **162**, 537–545.

5 (*a*) Y. F. Peng, S. Zhao, K. Li, L. Liu, B. L. Li and B. Wu, *CrystEngComm*, 2015, **17**, 2544–2552; (*b*) L. Liu, Y. F. Peng, X. X. Lv, K. Li, B. L. Li and B. Wu, *CrystEngComm*, 2016, **18**, 2490–2499; (*c*) L. L. Shi, T. R. Zheng, M. Li, L. L. Qian, B. L. Li and H. Y. Li, *RSC Adv.*, 2017, **7**, 23432–23443; (*d*) Q. Ding, Y. Pan, Y. Luo, M. Zhou, Y. Guan, B. Li, M. Trivedi, A. Kumar and J. Liu, *ACS Omega*, 2019, **4**, 10775–10783.

6 (*a*) X. Xiao, S. Tu, M. Lu, H. Zhong, C. Zheng, X. Zuo and J. Nan, *Appl. Catal., B*, 2016, **198**, 124–132; (*b*) Y. Wu, J. Wu, Z. Luo, J. Wang, Y. Li, Y. Han and J. Liu, *RSC Adv.*, 2017, **7**, 10415–10423; (*c*) H. Zhao, Q. Xia, H. Xing, D. Chen and H. Wang, *ACS Sustainable Chem. Eng.*, 2017, **5**, 4449–4456.

7 (*a*) C. Liao, Z. Ma, X. Chen, X. He and J. Qiu, *Appl. Surf. Sci.*, 2016, **387**, 1247–1256; (*b*) Y. Pan, Q. Ding, H. Xu, C. Shi, A. Singh, A. Kumar and J. Liu, *CrystEngComm*, 2019, **21**, 4578–4585.

8 (*a*) S. Demirci, T. Dikici, M. Yurddaskal, S. Gultekin, M. Toparli and E. Celik, *Appl. Surf. Sci.*, 2016, **390**, 591–601; (*b*) J. C. Jin, X. R. Wu, Z. D. Luo, F. Y. Deng, J. Q. Liu, A. Singh and A. Kumar, *CrystEngComm*, 2019, **19**, 4368–4377.

9 M. A. Rauf, M. A. Meetani, A. Khaleel and A. Ahmed, *Chem. Eng. J.*, 2010, **157**, 373–378.
10 K. S. Asha, R. Bhattacharjee and S. Mandal, *Angew. Chem., Int. Ed.*, 2016, **55**, 11528–11532.
11 (*a*) X. F. Lu, P. Q. Liao, J. W. Wang, J. X. Wu, X. W. Chen, C. T. He, J. P. Zhang, G. R. Li and X. M. Chen, *J. Am. Chem. Soc.*, 2016, **138**, 8336–8339; (*b*) J. Q. Liu, Z. D. Luo, Y. Pan, A. K. Singh, M. Trivedi and A. Kumar, *Coord. Chem. Rev.*, 2020, **406**, 213245; (*c*) M. L. Hu, Y. M. Mohammad and A. Morsali, *Coord. Chem. Rev.*, 2019, **387**, 415–435; (*d*) J. Liu, W. Wang, Z. Luo, B. Li and D. Yuan, *Inorg. Chem.*, 2017, **56**, 10215–10219.
12 (*a*) K. G. Liu, F. Rouhani, H. Moghanni-Bavil-Olyaei, X. W. Wei, X. M. Gao, J. Z. Li, X. W. Yan, M. L. Hu and A. Morsali, *J. Mater. Chem. A*, 2020, **8**, 12975–12983; (*b*) J. J. Liu, J. N. Xiao, D. B. Wang, W. Sun, X. C. Gao, H. Y. Yu, H. T. Liu and Z. L. Liu, *Cryst. Growth Des.*, 2017, **17**, 1096–1102; (*c*) Z. Z. Jiang, P. Zhou, T. T. Xu, L. H. Fan, S. M. Hu, J. X. Chen and Y. B. He, *CrystEngComm*, 2020, **22**, 3424–3431; (*d*) K. G. Liu, X. M. Gao, T. Y. Liu, M. L. Hu and D. E. Jiang, *J. Am. Chem. Soc.*, 2020, **142**(40), 16905–16909.
13 (*a*) M. L. Hu, V. Safarifard, E. Doustkhah, S. Rostamnia, A. Morsali, N. Nouruzi, S. Beheshti and K. Akhbari, *Microporous Mesoporous Mater.*, 2018, **256**, 111–127; (*b*) X. X. Cheng, S. Hojaghani, M. L. Hu, M. H. Sadr and A. Morsali, *Ultrason. Sonochem.*, 2017, **37**, 614–622; (*c*) L. Lu, J. Wang, B. Xie, J.-Q. Liu, R. Yadav, A. Singh and A. Kumar, *New J. Chem.*, 2017, **41**, 3537–3542.
14 A. Dutta, A. Singh, X. X. Wang, A. Kumar and J. Q. Liu, *CrystEngComm*, 2020, **22**, 7736–7781.
15 (*a*) M. L. Hu, S. A. Razavi, M. Piroozzadeh and A. Morsali, *Inorg. Chem. Front.*, 2020, **7**, 1598–1632; (*b*) G. Tan, Y. Zhong, L. Yang, Y. Jiang, J. Liu and F. Ren, *Chem. Eng. J.*, 2020, **390**, 124446; (*c*) Y. Y. Zhong, X. S. Li, J. H. Chen, X. X. Wang, L. T. Wei, L. Q. Fang, A. Kumar, S. Z. Zhuang and J. Q. Liu, *Dalton Trans.*, 2020, **49**, 11045–11058.
16 (*a*) Y. M. Lu, Y. Q. Lan, Y. H. Xu, Z. M. Su, S. L. Li, H. Y. Zang and G. J. Xu, *J. Solid State Chem.*, 2009, **182**, 3105–3112; (*b*) S. Y. Zhang, B. Liu, J. Yang, S. H. Zhang and K. F. Yue, *J. Solid State Chem.*, 2019, **273**, 141–149.
17 B. Kesanli, Y. Cui, M. R. Smith, E. W. Bittner, B. C. Bockrath and W. Lin, *Angew. Chem., Int. Ed.*, 2005, **44**, 72–75.
18 S. Aitipamula and A. Nangia, *Chem. Commun.*, 2005, 3159–3161.
19 (*a*) Y. Liu, X. L. Wang, J. Zhao, H. Y. Lin, N. Xu, J. W. Zhang and B. Y. Yu, *CrystEngComm*, 2019, **21**, 6613–6622; (*b*) H. Y. Lin, Z. W. Cui, Y. Tian, X. Wang and G. C. Liu, *J. Inorg. Organomet. Polym. Mater.*, 2018, **28**, 1810–1820; (*c*) M. Roy, S. Sengupta, S. Bala, S. Bhattacharya and R. Mondal, *Cryst. Growth Des.*, 2016, **16**, 3170–3179.
20 Y. S. Shi, D. Liu, L. S. Fu, Y. H. Lia and G. Y. Dong, *CrystEngComm*, 2020, **22**, 4079–4093.
21 F. Y. Yi, M. Gu, S. C. Wang, J. Q. Zheng, L. Pan and L. Han, *Inorg. Chem.*, 2018, **57**, 2654–2662.
22 Y. Y. Sun, X. J. Chen, F. Y. Wang, R. Ma, X. M. Guo, S. W. Sun, H. D. Guo and E. V. Alexandrov, *Dalton Trans.*, 2019, **48**, 5450–5458.
23 M. L. Han, J. G. Wang, L. F. Ma, H. Guo and L. Y. Wang, *CrystEngComm*, 2012, **14**, 2691–2701.
24 H. Y. Lin, J. Chi, S. Liang, M. Ji and G. C. Liu, *Z. Anorg. Allg. Chem.*, 2020, **646**, 514–522.
25 (*a*) H. J. Cheng, H. X. Tang, Y. L. Shen, N. N. Xia, W. Y. Yin, W. Zhu, X. Y. Tang, Y. S. Ma and R. X. Yuan, *J. Solid State Chem.*, 2015, **232**, 200–206; (*b*) K. G. Liu, F. Rouhani, X. M. Gao, M. Abbasi-Azad, J. Z. Li, X. D. Hu, W. Wang, M. L. Hu and A. Morsali, *Catal. Sci. Technol.*, 2020, **10**, 757–767.
26 (*a*) C. C. Wang, J. R. Li, X. L. Lv, Y. Q. Zhang and G. S. Guo, *Energy Environ. Sci.*, 2014, **7**, 2831–2867; (*b*) C. G. Silva, A. Corma and H. García, *J. Mater. Chem.*, 2010, 3141–3156; (*c*) A. Corma, H. García and F. X. L. Xamena, *Chem. Rev.*, 2010, **110**, 4606–4655.
27 H. H. Li, X. H. Zeng, H. Y. Wu, X. Jie, S. T. Zheng and Z. R. Chen, *Cryst. Growth Des.*, 2015, **15**, 10–13.
28 M. Nourian, F. Zadehahmadi, R. Kardanpour, S. Tangestaninejad, M. Moghadam, V. Mirkhani, I. Mohammadpoor-Baltork and M. Bahadori, *Catal. Commun.*, 2017, **94**, 42–46.
29 (*a*) T. R. Zheng, L. L. Qian, M. Li, Z. X. Wang, K. Li, Y. Q. Zhang, B. L. Li and B. Wu, *Dalton Trans.*, 2018, **47**, 9103–9113; (*b*) Y. G. Abou El-Reash, M. Otto, I. M. Kenawy and A. M. Ouf, *Int. J. Biol. Macromol.*, 2011, **49**, 513–522; (*c*) L. Wang, W. Liu, T. Wang and J. Ni, *Chem. Eng. J.*, 2013, **225**, 153–163.
30 L. L. Qian, Z. X. Wang, L. M. Zhu, K. Li, B. L. Li and B. Wu, *Spectrochim. Acta, Part A*, 2019, **214**, 372–377.
31 W. M. Cai, J. J. Chen, Q. W. Wang and M. Wei, *Water Sci. Technol.*, 2017, **76**, 3220–3226.
32 S. F. Chen, S. Zhang, T. Y. Wang, Z. Y. Lei, M. Q. Zhu, X. X. Dai, F. Liu, J. S. Li and H. Yin, *Mater. Chem. Phys.*, 2018, **208**, 258–267.
33 (*a*) J. C. Jin, J. Wu, W. C. Liu, A. Q. Ma, J. Q. Liu, A. Singh and A. Kumar, *New J. Chem.*, 2018, **42**, 2767–2775; (*b*) J. C. Jin, X. R. Wu, Z. D. Luo, F. Y. Deng, J. Q. Liu, A. Singh and A. Kumar, *CrystEngComm*, 2017, **19**, 4368–4377; (*c*) Y. Pan, Q. J. Ding, H. J. Xu, C. Shi, A. Singh, A. Kumara and J. Q. Liu, *CrystEngComm*, 2019, **21**, 4578–4585; (*d*) J. C. Jin, J. Wu, Y. X. He, B. H. Li, J. Q. Liu, R. Prasad, A. Kumar and S. R. Batten, *CrystEngComm*, 2017, **19**, 6464–6472; (*e*) F. Yuan, Y. Lia, X. Y. Ling, C. M. Yuan, C. S. Zhou, J. Wang, A. Singh, A. Kumar and F. Y. Chen, *Inorg. Chem. Commun.*, 2019, **109**, 107576; (*f*) C. P. Li, L. Lu, J. Wang, Q. Q. Yang, D. Y. Ma, A. Alowais, A. Alarifi, A. Kumar and M. Muddassir, *RSC Adv.*, 2019, **9**, 29864–29872; (*g*) Y. Wu, J. Wu, Z. D. Luo, J. Wang, Y. L. Li, Y. Y. Han and J. Q. Liu, *RSC Adv.*, 2017, **7**, 10415–10423; (*h*) A. K. Paul, G. Madras and S. Natarajan, *Phys. Chem. Chem. Phys.*, 2009, **11**, 11285–11296; (*i*) F. Yuan, C. M. Yuan, C. S. Zhou, C. F. Qiao, L. Lu, A. Q. Ma, A. Singh and A. Kumar, *CrystEngComm*, 2019, **21**, 6558–6565.
34 A. Bhattacharjee and M. Ahmaruzzaman, *J. Photochem. Photobiol., A*, 2018, **353**, 215–228.
35 I. Deganoa, F. Sabatini, C. Braccini and M. P. Colombini, *Dyes Pigm.*, 2019, **160**, 587–596.